Majority of Ruptures in Large Continental Strike-Slip Earthquakes Are Unilateral: Permissive Evidence for Hybrid Brittle-to-Dynamic Ruptures

Peter Bird*1 and Ross S. Stein²

Abstract

Finite-element models of neotectonics require transform faults to rupture seismically even where preseismic shear stresses are low, presumably by dynamic-weakening mechanisms. A long-standing objection is that, if a rupture initiated at an asperity with high static friction stresses, which then transitioned to low dynamic-weakening stresses, local stress drop would be near total and on the order of 80 MPa, which is $4\times-40\times$ greater than observed. But the 5 $M_{\rm w} \geq 7.8$ transform earthquakes since 2000 initially ruptured on the branch faults of small net slip (Stein and Bird, 2024). If the slip initiates on a branch fault with different slip physics and no dynamic weakening, this solves the stress-drop problem. We propose that most large shallow earthquakes are hybrid ruptures, which begin on branch faults of small slip with high shear stresses, and then continue propagating on a connected dynamically weakened fault of large slip, even where shear stresses are low. One prediction of this model is that most large shallow ruptures should be unilateral. We test this prediction against the 100 largest ($m \ge 6.49$) shallow continental strike-slip earthquakes 1977–2022, using information from the Global Centroid Moment Tensor and International Seismological Centre catalogs. The differences in time and location between the epicenter and the epicentroid define a horizontal "migration" velocity vector for the evolving centroid of each rupture. Early aftershock locations are summarized by a five-parameter elliptical model. Using the geometric relations between these (and mapped traces of active faults) and guided by a symmetrical decision table, we classified 55 ruptures as apparently unilateral, 30 as bilateral, and 15 as ambiguous. Our finding that a majority (55%-70%) of these ruptures are unilateral permits the interpretation that a majority of ruptures are hybrids, both in terms of geometry (branch fault to transform) and in terms of the physics of their fault slip.

Cite this article as Bird, P., and R. S. Stein (2024). Majority of Ruptures in Large Continental Strike-Slip Earthquakes Are Unilateral: Permissive Evidence for Hybrid Brittle-to-Dynamic Ruptures, *Seismol. Res. Lett.* **95**, 3306–3315, doi: 10.1785/0220240172.

Supplemental Material

Observations and Theoretical Problems That Motivate This Study

Faults of small net slip have been studied in rock-mechanics labs for decades, and it is well known that they obey Mohr–Coulomb friction theory (e.g., Engelder, 1993). Byerlee (1978) summarized lab results showing that virtually all the rocks have friction coefficient of ~0.85 at effective normal stresses up to 250 MPa, which corresponds to seismogenic depths of ~15 km in continental strike-slip faults with hydrostatic pore pressure. A few minerals like montmorillonite (Bird, 1984) and talc (Moore and Rymer, 2007; Collettini *et al.*, 2009; Moore and Lockner, 2011) have lower friction coefficients that may dominate in certain creeping faults, but are unlikely to be abundant and widespread enough to control crustal friction in all the

continents. Dieterich (1978, 1979, 1981) extended Mohr–Coulomb theory to create "rate and state friction" theory by modeling the small slip-rate dependence of friction coefficients, and also the ingrowth of cohesion with time on faults that do not slip, leading to improved predictions of seismic stress drop on such "Byerlee-type" faults (Fig. 1) in a model that only added two new parameters: a and b for any finite-size patch on a fault surface.

^{1.} Department of Earth, Planetary, and Space Sciences, University of California, Los Angeles, California, U.S.A., https://orcid.org/0000-0001-9034-1287 (PB);

^{2.} Temblor, Inc., Tiburon, California, U.S.A.

^{*}Corresponding author: pbird@epss.ucla.edu

[©] Seismological Society of America

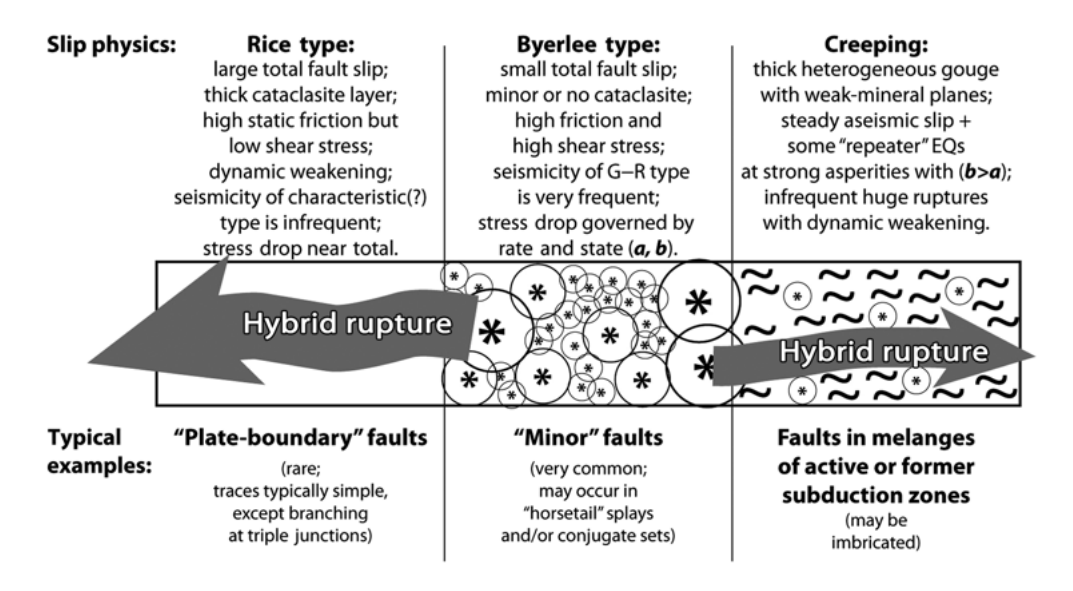


Figure 1. Suggested division of shallow continental fault surfaces by the physics of slip, into Byerlee type, Rice type, and creeping faults. All spatial dimensions are hypothetical. When a single earthquake rupture crosses a boundary between different domains of slip physics, we refer to it as a "hybrid rupture." Abbreviations: EQ, earthquake; G–R, Gutenberg–Richter. The "weak minerals" mentioned in the Creeping fault-physics section are probably talc and/or montmorillonite, as discussed in the text. Parameters *a* and *b* refer to the rate-and-state friction theory of Dieterich (1978, 1979, 1981). See Noda and Lapusta (2013) regarding infrequent huge ruptures with dynamic weakening on creeping faults.

About three decades ago, thin-plate (and thin-shell) finiteelement (F-E) modeling codes became available for the simulation of neotectonics, using actual topography, laterally varying heat flow, laterally varying crust and mantle-lithosphere thicknesses, actual fault maps, and realistic nonlinear flow laws of friction at low temperatures and dislocation creep at high temperatures, with different flow laws for crust and mantle (e.g., Bird, 1999; Bird et al., 2008). Figure 2 lists eight published studies of active tectonic regions, or of the whole Earth. Invariably, it was found that "Byerlee's law" friction gives a good representation of the relatively strong crustal blocks between modeled faults. However, in each case it was also found that successful models require the effective coefficient of friction on modeled faults (of large net slip) to be only ~0.03-0.17 in these quasi-static models that do not attempt to simulate earthquakes. These values are too low to be explained by montmorillonite/talc rocks in all the modeled fault zones, even if that were petrologically plausible.

The most plausible explanation is that these faults (of large slip) only move during earthquakes in which dynamic weakening is effective (Lapusta and Rice, 2003; Rice, 2006, 2017). One pervasive form of dynamic weakening is the heating of pore fluids by frictional work in the rock matrix, causing these fluids to expand and increase their pressure. That reduces the effective normal stress on the fault to low values, allowing slip to occur even where the preseismic shear traction on the fault was far below the level needed for Byerlee-type slip

initiation with normal hydrostatic pore pressure (Sibson, 1973; Lachenbruch and Sass, 1980; Rice, 2006, 2017; Noda *et al.*, 2009).

A plausible geologic basis for the distinction between Byerlee-type and Rice-type faults (Fig. 1) is that Rice-type faults have thick cataclasite layers resulting from their large net slips (Shipton et al., 2006). Thick cataclasite enhances dynamic weakening in two ways: (1) fault cataclasite is a low-velocity zone relative to the undeformed host rock (Faulkner et al., 2006; Li and Malin, 2008), and this lowvelocity zone focuses amplitude and energy of seismic waves from early parts of the rupture onto the adjacent parts of the fault plane, helping slip begin by dynamic triggering; (2) fault cataclasite has a

higher water content than undeformed host rock, because of (a) crystallographic water in the structure of some hydrated clays (e.g., Bird, 1984); (b) hydration spheres of weakly structured water held around tiny silicate grains by Van der Waals bonding (Byerlee, 1990); and (c) additional free pore space in which pore-fluid flow obeys Darcy's law. Abundant water means that mechanisms involving thermal expansion of pore fluids are more plausible and cannot be easily dismissed based on arguments anticipating rapid diffusion of pore pressure.

A long-standing problem with this model of dynamically weakened transform faults is that it seems to predict occasional huge stress drops on the fault segments where ruptures initiate; but such huge stress drops are not observed. For example, at a median depth of 6 km in the seismogenic portion of a continental strike-slip fault, the effective normal stress (reduced by hydrostatic pore pressure) is about 98 MPa. Assuming a typical Byerlee friction coefficient of 0.85 (appropriate to these low pressures), the shear stress at initiation of sliding would be at least 83 MPa. That means we would expect a mean seismic stress drop on the order of 80 MPa for that fault segment after dynamic weakening occurs. Yet such huge stress drops are rarely (or never?) observed in large shallow earthquakes. The systematic compilation of Kanamori and Anderson (1975) showed stress drops of 1-8 MPa among "interplate" earthquakes (i.e., those occurring on faults of large net slip). Even among their "intraplate" earthquakes (i.e., those occurring on previously unknown faults) the highest stress drop was 20 MPa. A later

Mean effective fault friction (defined for quasi-static slip and hydrostatic pore pressure) inferred in F-E dynamic-modeling studies

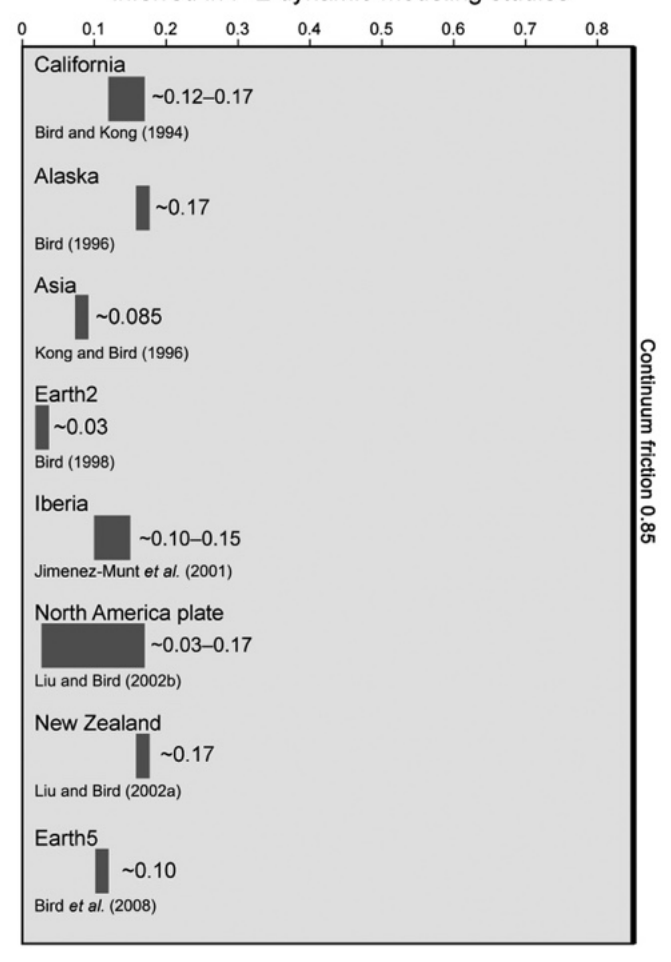


Figure 2. Graphical summary of effective friction coefficients (defined for quasi-static slip and hydrostatic pore pressure) inferred in eight neotectonic-dynamics modeling studies with the Faults/Plates/Shells family of finite-element (F-E) programs by the first author. Abbreviations Earth2 and Earth5 represent global lithosphere models at different spatial resolutions. All optimal coefficients for the modeled faults are significantly less than "Byerlee's law" friction of 0.85, requiring that some dynamic-weakening process is active in modeled faults (but not in the continuum between them). In that case, each of these effective friction coefficients can be interpreted as one-half of the ratio of preseismic shear traction to preseismic effective normal stress on the modeled faults.

study by Richardson and Solomon (1977) showed stress drops of 0.2–10 MPa on both interplate and intraplate faults. A comprehensive study of California earthquakes (mostly small) by Shearer *et al.* (2006) found the stress drops of 0.2–20 MPa with a median of 2 MPa, independent of magnitude. A related problem is that such an exceptionally high stress drop would be accompanied by very large slip-per-event, which has not yet been seen in the paleoseismic records of well-studied regions like California and Türkiye.

A solution is possible where the faults of large slip intersect branch faults (of small net slip) in horsetail splays, unstable triple junctions (McKenzie and Morgan, 1969), and/or ancestral process zones. The rupture may begin on a Byerlee-type branch fault (where there is high shear traction but no dynamic weakening), and then continue onto the connected Rice-type fault with dynamic weakening (but low ambient preseismic shear stress). The stress drop on the initiating branch fault would be determined by the parameters a and b of rate and state friction theory and would be modest. The stress drop on the Rice-type fault would be limited to ambient preseismic shear stress, which F-E modeling indicates is also modest. In Figure 1, and below, we refer to ruptures that change their slipphysics midearthquake as "hybrid ruptures."

Stein and Bird (2024) present an analysis of published studies showing that all of the great (m > 7.8) continental strike-slip earthquakes since 2000 began on the branch faults of small net slip, before expanding greatly on more famous faults of large net slip. Although this topological phenomenon does not directly constrain slip physics, it is strongly suggestive of a transition in physics such as we have suggested here.

If the great majority of large shallow earthquakes involve "plate-boundary" or other "major" Rice-type faults of large net slip and thick cataclasite, and if each of these earthquakes must initiate on a Byerlee-type branch fault of small net slip but high shear traction, then these earthquakes should have hybrid ruptures. In addition, there are reasons to expect that a branch-fault rupture intersecting a transform fault in a λ -shaped nexus should typically propagate only in the "forward" direction (i.e., making an acute-angle bend) rather than in the "backward" direction (i.e., making an obtuse-angle bend). Quasi-static Coulomb stress transfer models support this. It is also the typical result in fully dynamic rupture models (Poliakov et al., 2002). And, a detailed field study of the Altyn Tagh fault by Elliott et al. (2015) shows that angles greater than 18° are often the barriers to rupture propagation. If propagation onto the transform is one sided, and the transform is long compared to the branch fault rupture, we further predict that most of these hybrid ruptures should be essentially unilateral ruptures (Fig. 1). This concept is supported by the McGuire et al. (2002) study of second moments of 25 shallow m > 7 earthquakes worldwide; they found that ~80% of these ruptures are "predominantly unilateral."

In the present study, we extend the classification of shallow ruptures as unilateral or bilateral to smaller magnitudes ($m \ge 6.49$), allowing us to form a larger test subcatalog of 100 events, even as we restrict consideration to only continental strike-slip events.

This contribution is intended to honor our former colleagues and coauthors David D. Jackson and Yan Y. Kagan of the University of California, Los Angeles. From Jackson we take the idea that the best way to begin testing a hypothesis about earthquakes is to sample the greatest possible number (e.g.,

all those in some class) and to use data from the respected thirdparty sources (e.g., seismic catalogs). From Kagan we take an elegant method (Kagan, 2002) for objectively describing the map pattern of early aftershocks with a five-parameter ellipse, and its use as a proxy for the rupture length and location.

New Research

In this project, we study large shallow continental strike-slip earthquakes, for three reasons: (1) continental earthquakes are more likely to occur in places where traces of active faults have been mapped; (2) continental earthquakes are more likely to be recorded at nearby seismic stations, permitting more accurate estimates of epicenter, epicentroid, and aftershock locations; and (3) depth is typically the least precise parameter in event locations, so we prefer a map view of spatial relations (i.e., looking downward), and strike-slip events are most easily understood in map view.

We sampled the Global Centroid Moment Tensor (Global CMT) catalog (see Data and Resources), years 1977–2022, for shallow ($z \le 70 \text{ km}$) events that had a positive surface elevation at their epicentroid, and which had the intermediate (B) axis of their focal mechanism plunging more steeply than either the compressional (P) or tensile (T) axes. This means that we included some oblique-slip events, as long as their strike-slip component was dominant. The result was 100 events with $m \ge 6.49$. These events are listed, in descending order by magnitude, in attached file Supplement-Table_1.xlsx, available in the supplemental material of this article. All magnitudes m mentioned in this article are moment magnitudes on the U.S. Geological Survey scale.

Each Global CMT event solution includes an epicenter (often from the National Earthquake Information Center catalog) and an epicentroid. The epicentroid is the surface point overlying the hypocentroid, which is the point source (both in space and time) best approximating the actual finite rupture. The epicenter can be thought of as the surface point overlying the approximate center of the rupture when the earthquake first reached the catalog-completeness magnitude (i.e., $m \cong 4$), and the epicentroid is the surface point overlying the center of the completed rupture. The horizontal movement from the epicenter to the epicentroid (both in space and in time) is here called "migration." The ratio of the migration distance to the migration time is the "migration velocity." Migration velocity is useful in distinguishing bilateral from unilateral ruptures. In a symmetric bilateral rupture, the migration distance is nearly zero, but the migration time is positive, so the migration velocity is small. However, for a unilateral rupture, the migration velocity is approximately (half the final rupture length)/(half the rupture time), and thus comparable to the rupture velocity. Rupture velocity is typically close to the Rayleigh wavespeed, at ~92% of shear velocity (except for supershear ruptures, which are faster). Therefore, as an initial discriminator for

bilateral/unilateral ruptures, we use a critical velocity which is one-half the Rayleigh velocity, or 1.62 km/s in typical continental crust.

Another useful measure of rupture length and location is the distribution of early aftershock epicenters. We selected potential early aftershocks from the International Seismological Centre (ISC) catalog (see Data and Resources) by automated queries and recorded them with the Wget utility.

A minimum or threshold magnitude was one criterion for inclusion of a potential aftershock. Kagan (2002) used a lower magnitude limit of 4.5 because it was the global completeness threshold for the years of ISC catalog that he sampled. We adopted a lower threshold magnitude of 4.0 based on the argument that continental aftershocks typically occur closer to seismometers and thus can be reliably detected to a slightly lower magnitude.

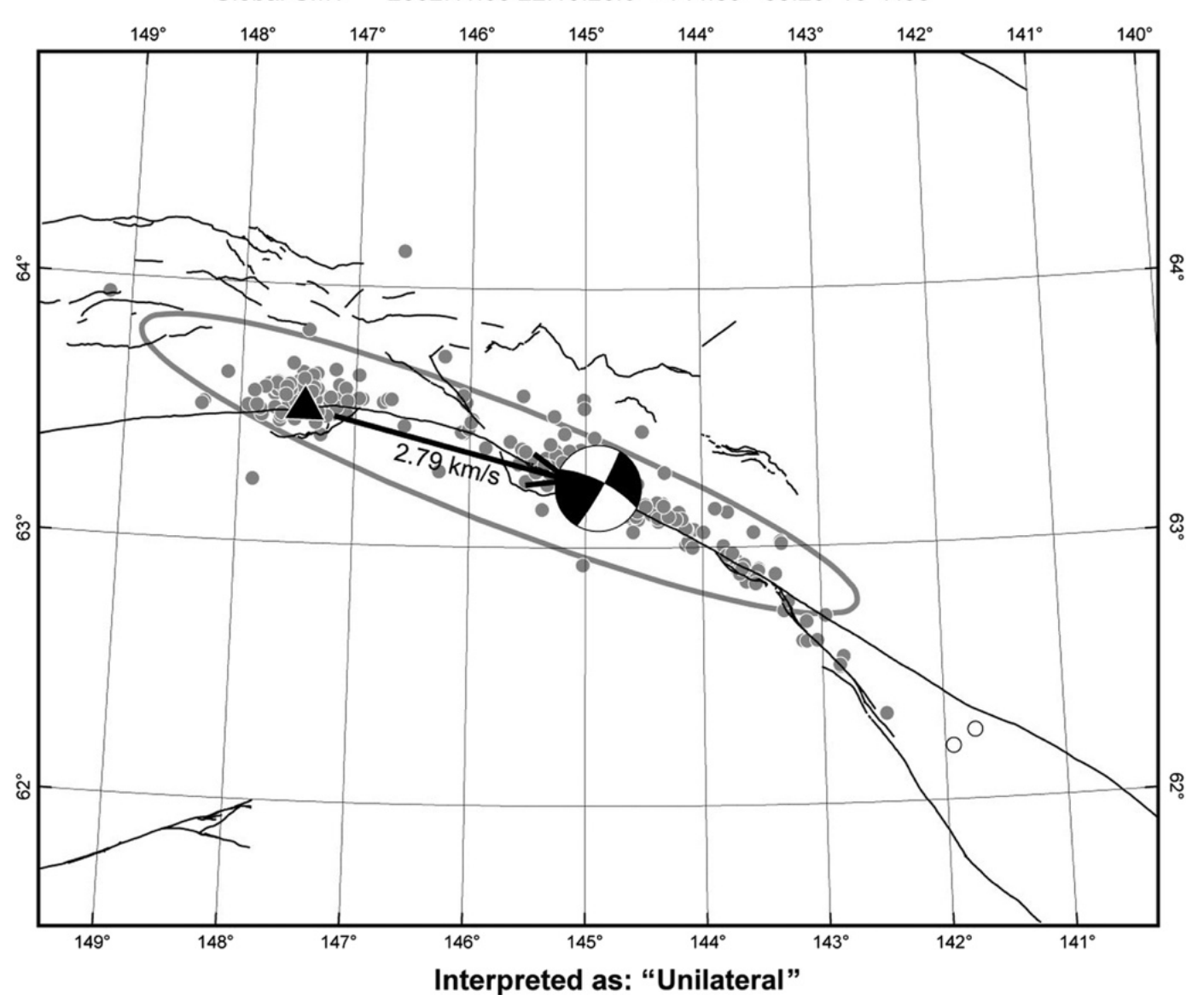
Along the time axis, a second criterion for potential early aftershocks was a duration of 1 week or less. Our time window of 1 week was also based on the study of Kagan (2002), who also experimented with an alternative time window of 1 day. Because our study includes magnitudes down to 6.49, whereas Kagan's study was limited to $M_{\rm w}$ 7+; the longer time window seems appropriate to collect sufficient early aftershocks. However, there were eight cases in which a second large shock followed in the same region within the week; in those cases, we manually truncated the time window to exclude secondary aftershocks of these large, triggered ruptures.

In designing the spatial criterion for inclusion of potential early aftershocks, we needed to avoid biasing our results in favor of either bilateral or unilateral rupture. Simplistically, we expected that early aftershocks from a bilateral rupture might be symmetric about the epicenter, so the distance from the epicenter could be a criterion. However, in a unilateral rupture the early aftershocks might all be to one side of the epicenter but perhaps symmetrically distributed about the epicentroid. Therefore, our rule was that the potential aftershock must have its epicenter less than a critical distance from either the epicenter or the epicentroid. This critical distance was the "Kagan radius" of $r = (20 \text{ km}) \ 10^{[(m-6)/2]}$ (Kagan, 2002).

Following Kagan (2002), we also computed a five-parameter ellipse (in the horizontal plane) that best represents the distribution of aftershocks. This ellipse could be interpreted as locating the rupture, especially when its aspect ratio is large.

For each of the 100 events in our subcatalog, we produced an automated map showing: coastlines, plate boundaries of Bird (2003), the traces of active faults from Styron and Pagani (2020), the focal mechanism of the mainshock from Global CMT, the migration vector labeled with migration velocity, the early aftershock epicenters, and the ellipse summarizing the positions of the early aftershocks. This map was the basis for our decision as to whether each rupture was apparently unilateral (e.g., Fig. 3), bilateral (e.g., Fig. 4), or ambiguous (e.g., Fig. 5).

Susitna Glacier-Denali-Totschunda, Alaska, U.S.A. Global CMT 2002.11.03 22:13:28.0 -144.89 63.23 15 7.88



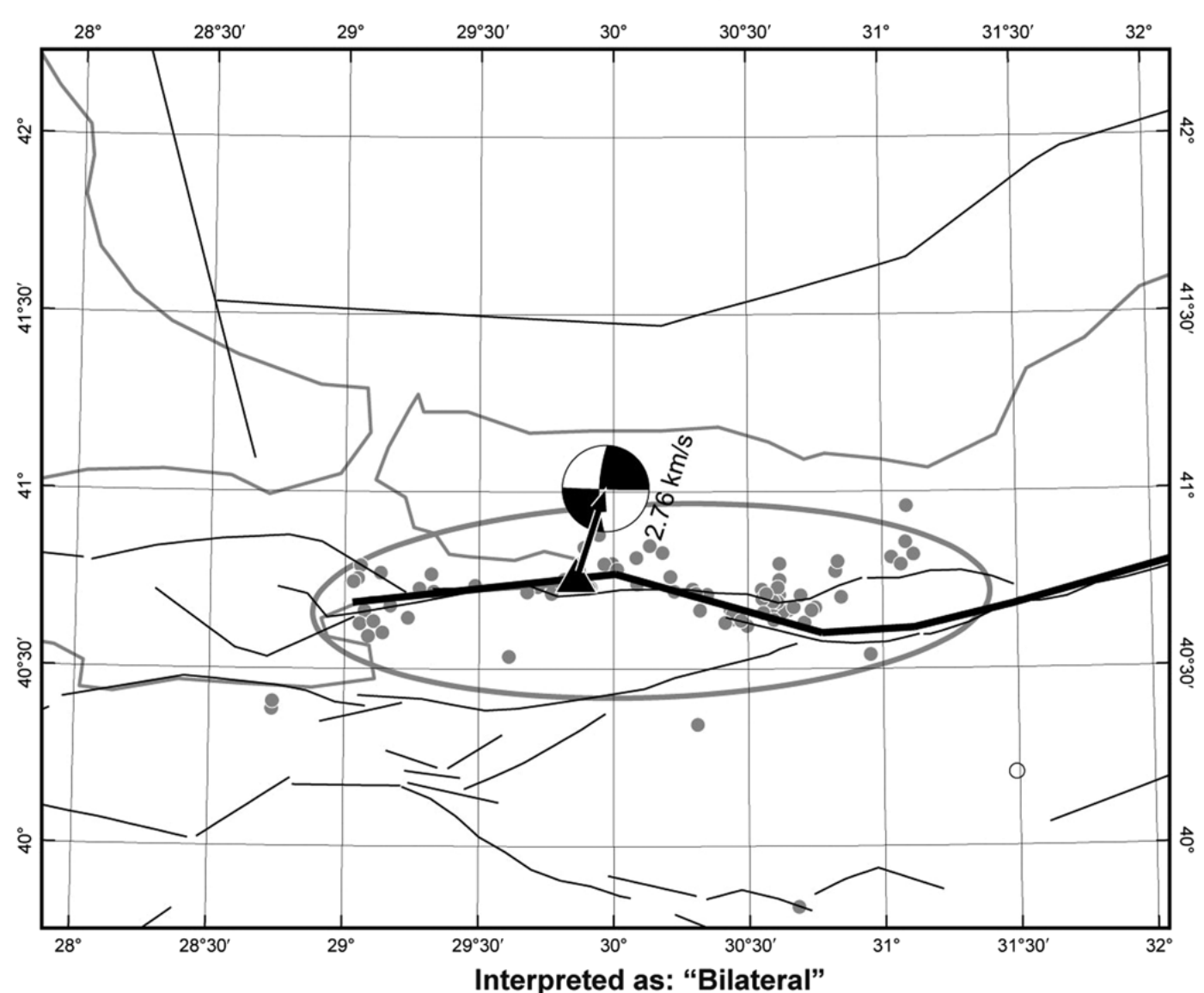
A PDF document containing images of all the 100 event-specific rupture maps is attached as file Supplement-100_Earthquake_Rupture_Maps.pdf.

The preceding examples (especially Figs. 4 and 5) show that sometimes the indications from the migration-velocity discriminator and the aftershock-distribution discriminator do not agree. Another consideration is whether the migration-velocity vector is parallel to the mapped traces of active faults (where available) or parallel to the trend of aftershocks (when available); a migration vector that is orthogonal to the mapped traces and/or aftershock trends is inherently implausible and may be an artifact due to different catalog-dependent biases affecting the epicenter and the epicentroid differently.

To clarify our classification decisions, we adopted the decision matrix shown in Figure 6. One goal in designing this matrix was to avoid any bias toward any particular outcome.

Figure 3. Sample map of a continental strike-slip earthquake that we classified as a unilateral rupture. This example is the *m* 7.88 Susitna Glacier–Denali–Totschunda earthquake of 3 November 2002 in Alaska. Traces of active faults from Styron and Pagani (2020) shown with thin black lines. Epicenter from Global Centroid Moment Tensor (Global CMT) (which obtained it from National Earthquake Information Center shown with black triangle. Epicentroid from Global CMT shown with a focal mechanism on lower focal hemisphere. The migration vector is shown with a heavy black arrow from epicenter to epicentroid and is labeled with migration velocity (if greater than 1.62 km/s). Early aftershocks from ISC are shown with small gray circles. The ellipse summarizing early aftershock locations (Kagan, 2002) is shown with a heavy gray curve.

Izmit earthquake, Türkiye Global CMT 1999.08.17 00:01:50.1 29.97 41.01 17 7.61



Accordingly, we gave the matrix an overall monoclinic symmetry, with equal numbers of cells labeled as Unilateral, Bilateral, and Ambiguous (three of each).

Each cell in Figure 6 also shows the fraction of our 100 test earthquakes that were assigned to that cell. Adding related totals, the estimated fraction of unilateral ruptures is 33% + 19% + 3% = 55%. The estimated fraction of bilateral ruptures is 17% + 8% + 5% = 30%. The fraction of ruptures that remain ambiguous is 9% + 5% + 1% = 15%.

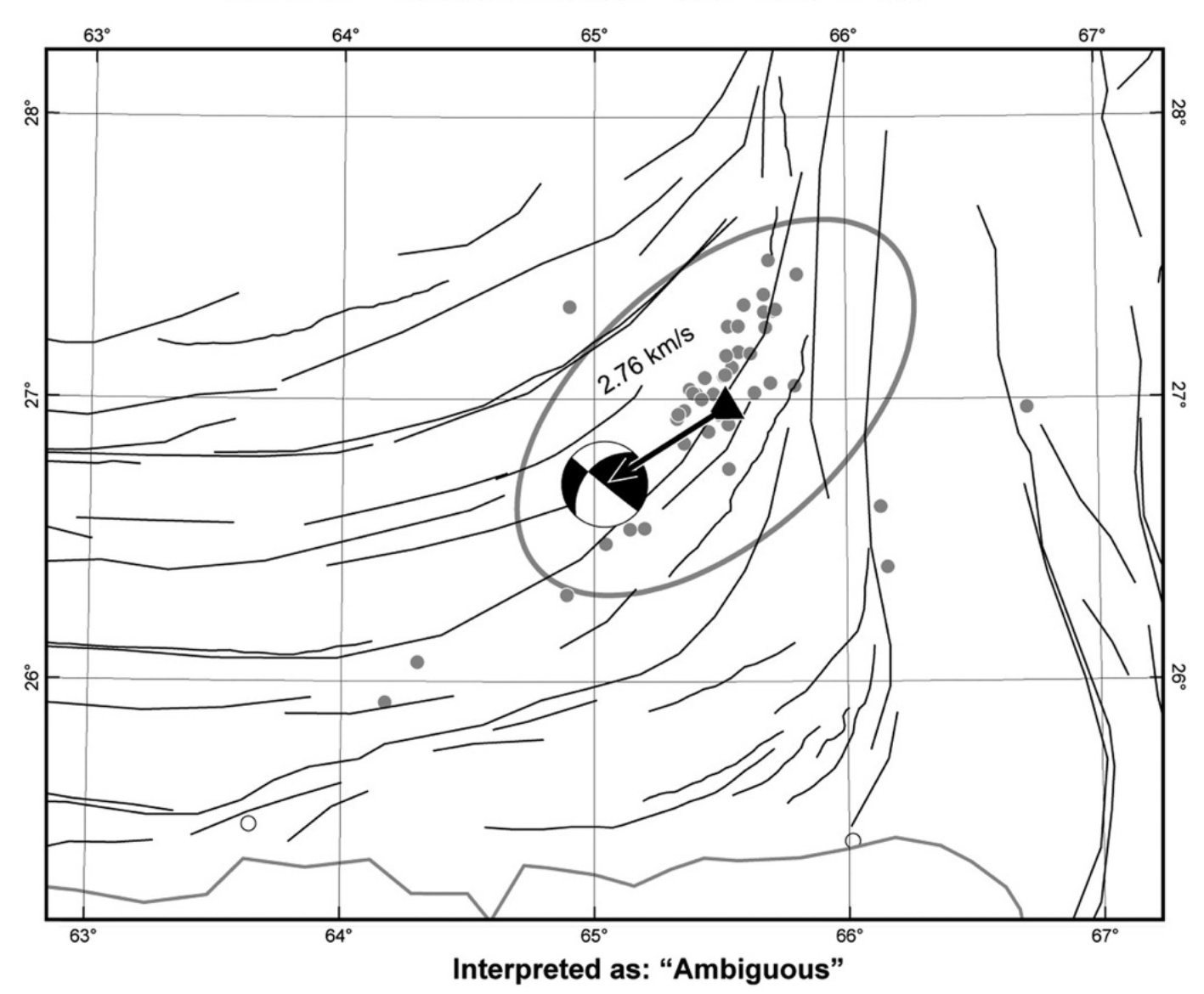
Conclusions and Further Hypotheses

Our classification of the 100 largest (*m* 6.49+) shallow continental strike-slip earthquakes during 1977–2022 resulted in a finding that unilateral ruptures were 55%–70%, whereas bilateral ruptures were 30%–45%. Despite the uncertainty resulting from ambiguous cases, we find that a majority

Figure 4. Sample map of a continental strike-slip earthquake that we classified as a bilateral rupture. This example is the *m* 7.61 Izmit earthquake of 17 August 1999 in Türkiye. Graphical conventions as in Figure 3. In this case, the migration velocity was large but the migration direction was orthogonal to mapped traces of active faults, and therefore implausible. In addition, the distribution of early aftershocks was symmetrical about the epicenter.

of these ruptures were unilateral. This is consistent with the concepts developed in our introduction, especially the idea that most of the ruptures along "plate-boundary" and other "major" faults (of large net slip, with thick cataclasite, and effective dynamic weakening) must originate on a connected Byerlee-type branch fault of small net slip and high shear stress, and then develop into hybrid ruptures (as schematically shown in Fig. 1).

SW Pakistan (Balochistan) {oblique} Global CMT 2013.09.24 11:30:08.4 65.04 26.70 12 7.80



It is also necessary to consider a natural objection: if the concepts in our introduction are correct, then why was the fraction of unilateral ruptures not higher? Specifically, why was our estimate of this fraction less than the estimate (80%) that McGuire *et al.* (2002) found for *m* 7+ earthquakes worldwide, in all the tectonic regimes? Here, we can suggest two additional hypotheses that may be relevant:

1. In places where a new continental shear zone is forming, there may be only young Byerlee-type faults of small net slip. If there is no "major" Rice-type transform fault (of large net slip) for them to connect with, then these ruptures would not be able to develop into hybrid ruptures, and there would be no reason to expect them to be unilateral. Domestic examples from our data set include the *m* 6.50 Monte Cristo Range earthquake of 15 May 2020 in Nevada,

Figure 5. Sample map of a continental strike-slip earthquake that we classified as an ambiguous rupture. This example is the m 7.80 Balochistan earthquake of 24 September 2013 in Pakistan. Graphical conventions as in Figure 3. In this case, the migration velocity was large and roughly parallel to the traces of active faults, but the distribution of early aftershocks was roughly symmetrical about the epicenter. This rupture was classified as Ambiguous because of these conflicting indicators.

the m 7.06 Ridgecrest earthquake of 6 July 2019 in California, and the m 7.15 Hector Mine earthquake of 16 October 1999 in California. Furthermore, there is a reason to think that this situation of changing fault geometry may be more common at smaller length scales associated with smaller magnitudes. Many small (e.g., m < 4) aftershocks appear to occur near, but not on, the master faults whose

		Aftershocks		
		Symmetrical around epicenter	None, few, or ambiguous	Mostly on one side of epicenter
M i g r	Slow (<1.62 km/s)	"Bilateral" (17%)	"Bilateral" (5%)	Migration direction opposite or perpendicular to aftershock direction: "Ambiguous" (5%) Migration direction matches aftershock direction: "Unilateral" (3%)
a t i	Fast (>1.62 km/s)	At right angles to fault trace: "Bilateral" (8%)	At right angles to fault trace: "Ambiguous" (1%)	"Unilateral" (33%)
o n		Parallel to fault trace, or when fault is unknown: "Ambiguous" (9%)	Parallel to fault trace, or when fault is unknown: "Unilateral" (19%)	

Figure 6. Our decision matrix, with (row) axis of migration velocity, and (column) axis of aftershock symmetry/asymmetry. Another consideration (in subcells) is whether the migration velocity was parallel to the fault traces and/or the aftershock lineament/ellipse, or perpendicular. Figures in parentheses show the fraction of the 100 events in our study that were assigned to each cell.

mainshock triggered them, and these are often thought to be related to tectonically short-term stress fields associated with nonplanar faults, fault bends, stepovers, and/or unstable triple junctions between major faults. This suggests the idea that the fraction of hybrid (and thus unilateral) ruptures should decline with declining magnitude, perhaps explaining the discrepancy between our estimate and that of McGuire *et al.* (2002). In this area, our ideas connect to those of Lee *et al.* (2024); specifically, we think that the very high shear stresses that permit Byerlee-type rupture initiation are more common where faults are complex, immature, and evolving.

2. In this study, we have assumed that a Byerlee-type rupture that intersects a Rice-type fault (Fig. 1) will continue in only one direction along that master fault, producing a unilateral rupture. As mentioned earlier, this assumption is supported by both dynamic-rupture modeling (Poliakov et al., 2002) and by a study of ruptures along the Altyn Tagh fault zone (Elliott et al., 2015). However, there is a counterexample: the Ren et al. (2024) study of the first (m 7.8) Kahramanmaraş, Türkiye, earthquake of 6 February 2023 found that it began on a minor branch fault (Nurdagi segment) as a possibly supershear rupture, then continued as a supershear rupture in both directions along the East Anatolian fault (to the northeast on the Pazarcik and Erkenek segments; to the southwest on the Amanos segment). Perhaps this was an unusual case because it involved supershear ruptures with different physics. However, it shows that some cases of macroscopically bilateral rupture may actually be hybrid ruptures

(starting on a branch fault of small net slip) when analyzed in detail. Thus, it is theoretically possible that the true fraction of hybrid ruptures could be slightly higher than the fraction of apparently unilateral ruptures that we have estimated.

The original hypothesis motivating this study was that earthquake ruptures on lightly stressed transform with Rice-type dynamic-weakening physics must begin as Byerlee-type ruptures highly stressed branch faults of small net slip. Our new result on the prevalence of unilateral ruptures in large shallow continental strike-slip earthquakes is far from providing proof of that hypothesis; it is

merely consistent or permissive evidence. However, we can suggest certain additional implications of our hypothesis for further investigation: (1) that Rice-type transforms (of large net slip) should be seismically quiet between large ruptures. That is, they should not display Gutenberg-Richter frequency-magnitude relations with lots of small earthquakes, but something more unimodal. Unfortunately, such a prediction is very difficult to test, because when the master fault is quiet it is also hard to locate, and it is therefore hard to separate out all Byerlee-type seismicity that might occur in the surrounding crustal blocks. (2) Ruptures on a particular Rice-type transform should not be periodic in time, because they are always triggered by a Byerlee-type rupture entering from a branch fault, rather than by the slow tectonic rise of shear tractions to any critical value. (3) Ruptures on a particular Ricetype transform, assuming that they have nearly complete stress drops due to dynamic weakening, should follow the slip-predictable rule; that is, slip released in a large earthquake should be roughly equal to virtual slip accumulated as an elastic strain since the last large earthquake on that same fault.

However, in future testing of these predictions, it will be critical to exclude fault segments with creeping-fault physics (Fig. 1). Such faults would be expected to have frequent small earthquakes at asperities on their surfaces, and some of these asperities even produce earthquakes that are periodic in time. Thus, future study of large earthquake ruptures should attempt to divide these earthquakes into three subcatalogs of events that were ruled by the three different types of slip physics outlined in Figure 1.

Data and Resources

Mainshocks from the Global Seismic Moment Tensor (Global CMT) catalog (Dziewonski et al., 1981; Ekström et al., 2012) were downloaded annually from https://www.ldeo.columbia.edu/~gcmt/projects/CMT/ catalog/NEW_MONTHLY/ (last accessed October 2023, covering calendar year 2022), as the sets of 12 monthly .NDK files. These .NDK files were then converted to .EQC files (which format is documented at http://peterbird.name/oldFTP/2003107-esupp/eqc_format.pdf, last accessed November 2023) using our utility program Seismicity, available from http://peterbird.name/oldFTP/Seismicity/ (last accessed November 2023). Early aftershocks for each of the 100 mainshocks were obtained from the International Seismological Centre (ISC) catalog (Bondár and Storchak, 2011; Storchak et al., 2017, 2020), using the automated command-line query feature presented at https://www.isc.ac.uk/iscbulletin/ search/webservices/ (last accessed November 2023). The results from the queries were recorded as computer files using the Wget utility, available from https://www.gnu.org/software/wget/ (last accessed November 2023). The supplemental material includes (1) Supplement-Table_1.xlsx (too wide for print format) describes the 100 earthquakes studied; and (2) Supplement-100_Earthquake_Rupture_Maps.pdf is a 100-page document including a regional map of faults and aftershocks surrounding each epicenter/epicentroid pair that we studied.

Declaration of Competing Interests

The authors acknowledge that there are no conflicts of interest recorded.

Acknowledgments

R. S. S. is grateful for funding to Temblor from the National Science Foundation through its Small Business Innovation Research program. The authors thank two anonymous reviewers for conceptual corrections and for supporting references.

References

- Bird, P. (1984). Hydration-phase diagrams and friction of montmorillonite under laboratory and geologic conditions, with implications for shale compaction, slope stability, and strength of fault cataclasite, *Tectonophysics* **107**, 235–260.
- Bird, P. (1996). Computer simulations of Alaskan neotectonics, *Tectonics* **15**, no. 2, 225–236.
- Bird, P. (1998). Testing hypotheses on plate driving mechanisms with global lithosphere models including topography, thermal structure, and faults, *J. Geophys. Res.* **103**, no. B5, 10,115–10,129.
- Bird, P. (1999). Thin-plate and thin-shell finite element programs for forward dynamic modeling of plate deformation and faulting, *Comput. Geosci.* **25**, no. 4, 383–394.
- Bird, P. (2003). An updated digital model of plate boundaries, *Geochem. Geophys. Geosys.* **4,** no. 3, 1027, doi: 10.1029/2001GC000252.
- Bird, P., and Y. Y. Kagan (2004). Plate-tectonic analysis of shallow seismicity: Apparent boundary width, beta, corner magnitude, coupled lithosphere thickness, and coupling in seven tectonic settings, *Bull. Seismol. Soc. Am.* **94**, no. 6, 2380–2399.
- Bird, P., and X. Kong (1994). Computer simulations of California tectonics confirm very low strength of major faults, *Geol. Soc. Am. Bull.* **106**, no. 2, 159–174.
- Bird, P., Z. Liu, and W. K. Rucker (2008). Stresses that drive the plates from below: Definitions, computational path, model optimization,

- and error analysis, *J. Geophys. Res.* **113**, no. B11, doi: 10.1029/2007[B005460.
- Bondár, I., and D. A. Storchak (2011). Improved location procedures at the International Seismological Centre, *Geophys. J. Int.* **186**, 1220–1244, doi: 10.1111/j.1365-246X.2011.05107.x.
- Byerlee, J. (1978). Friction in rocks, *Pure Appl. Geophys.* **116**, 615–626. Byerlee, J. (1990). Friction, overpressure, and fault normal compression, *Geophys. Res. Lett.* **17**, 2109–2112.
- Collettini, C., C. Viti, S. A. F. Smith, and R. E. Holdsworth (2009). Development of interconnected talc networks and weakening of continental low-angle normal faults, *Geology*, **37**, no. 6, 567–570, doi: 10.1130/G25645A.1.
- Dieterich, J. H. (1978). Time-dependent friction and mechanics of stick-slip, *Pure Appl. Geophys.* **116,** 790–806.
- Dieterich, J. H. (1979). Modeling of rock friction, 1: Experimental results and constitutive equations, *J. Geophys. Res.* **84**, 2161–2168.
- Dieterich, J. H. (1981). Constitutive properties of faults with simulated cataclasite, in *Mechanical Behavior of Crustal Rocks*, N. L. Carter, M. Friedman, J. M. Logan, and D. W. Stearns (Editors), Geophysical Monograph Series, Vol. 24, AGU, Washington DC, 103–120.
- Dziewonski, A. M., T.-A. Chou, and J. H. Woodhouse (1981). Determination of earthquake source parameters from waveform data for studies of global and regional seismicity, *J. Geophys. Res.* **86**, 2825–2852, doi: 10.1029/JB086iB04p02825.
- Ekström, G., M. Nettles, and A. M. Dziewonski (2012). The global CMT project 2004-2010: Centroid-moment tensors for 13,017 earthquakes, *Phys. Earth Planet. In.* **200-201**, nos. 1/9, doi: 10.1016/j.pepi.2012.04.002.
- Elliott, A. J., M. E. Oskin, J. Liu-Zeng, and Y. Shao (2015). Rupture termination at restraining bends: The last great earthquake on the Altyn Tagh fault, *Geophys. Res. Lett.* **42**, no. 7, 2164–2170.
- Engelder, T. (1993). Stress Regimes in the Lithosphere, Princeton University Press, Princeton, New Jersey, 457 pp.
- Faulkner, D. R., T. M. Mitchell, D. Healy, and M. J. Heap (2006). Slip on 'weak' faults by the rotation of regional stress in the fracture damage zone, *Nature* **444**, doi: 10.1038/nature05353.
- Jimenez-Munt, I., P. Bird, and M. Fernandez (2001). Thin-shell modeling of neotectonics in the Azores-Gibraltar region, *Geophys. Res. Lett.* **28**, no. 6, 1083–1086.
- Kagan, Y. Y. (2002). Aftershock zone scaling, *Bull. Seismol. Soc. Am.* **92,** no. 2, 641–655.
- Kanamori, H., and D. L. Anderson (1975). Theoretical basis of some empirical relations in seismology, *Bull. Seismol. Soc. Am.* **65**, 1073–1095.
- Kong, X., and P. Bird (1996). Neotectonics of Asia: Thin-shell finiteelement models with faults, in *The Tectonic Evolution of Asia*, A. Yin and T. M. Harrison (Editors), Cambridge University Press, Cambridge, United Kingdom, 18–34.
- Lachenbruch, A. H., and J. H. Sass (1980). Heat flow and energetics of the San Andreas fault zone, *J. Geophys. Res.* **85**, 6185–6222, doi: 10.1029/JB085iB11p06185.
- Lapusta, N., and J. R. Rice (2003). Low-heat and low-stress fault operation in earthquake models of statically strong but dynamically weak faults, *AGU Fall Meeting Abstracts*, San Francisco, California, Vol. 84, Abstract S51B-02.
- Lee, J., V. C. Tsai, G. Hirth, A. Chaterjee, and D. T. Trugman (2024). Fault-network geometry influences earthquake frictional behaviour, *Nature* doi: 10.1038/s41586-024-07518-6.

- Li, Y.-G., and P. E. Malin (2008). San Andreas fault damage at SAFOD viewed with fault-guided waves, *Geophys. Res. Lett.* **35**, L08304, doi: 10.1029/2007GL032924.
- Liu, Z., and P. Bird (2002a). Finite element modeling of neotectonics in New Zealand, *J. Geophys. Res.* **107**, no. B12, 2328, doi: 10.1029/2001JB001075.
- Liu, Z., and P. Bird (2002b). North America plate is driven westward by lower mantle flow, *Geophys. Res. Lett.* **29**, no. 24, 2164, doi: 10.1029/2002GL016002.
- McGuire, J. J., L. Zhao, and T. H. Jordan (2002). Predominance of unilateral rupture for a global catalog of large earthquakes, *Bull. Seismol. Soc. Am.* **92**, no. 8, 3309–3317.
- McKenzie, D. P., and W. J. Morgan (1969). Evolution of triple junctions, *Nature* **224**, no. 5215, 125–133.
- Moore, D. E., and D. A. Lockner (2011). Frictional strengths of talc-serpentine and talc-quartz mixtures, *J. Geophys. Res.* **116**, no. B1, doi: 10.1029/2010JB007881.
- Moore, D. E., and M. J. Rymer (2007). Talc-bearing serpentinite and the creeping section of the San Andreas fault, *Nature* **448**, 795–797, doi: 10.1038/nature06064.
- Noda, H., and N. Lapusta (2013). Stable creeping fault segments can become destructive as a result of dynamic weakening, *Nature* **493**, doi: 10.1038/nature11703.
- Noda, H., E. M. Dunham, and J. R. Rice (2009). Earthquake ruptures with thermal weakening and the operation of major faults at low overall stress levels, *J. Geophys. Res.* 114, no. B7, doi: 10.1029/ 2008JB006143.
- Poliakov, A. N. B., R. Dmowska, and J. R. Rice (2002). Dynamic shear rupture interactions with fault bends and off-axis secondary faulting, *J. Geophys. Res.* **107**, no. B11, ESE 6-1-ESE 6-18.
- Ren, C., W. Zhang, T. Wang, Z. Ge, T. Serkan Irmak, C. Erman, Y. Zhou, Z. Li, H. Xu, B. Cao, and H. Ding (2024). Supershear triggering and cascading fault ruptures of the 2023 Kahramanmaras, Turkiye, earthquake doublet, *Science* 383, no. 6680, 305–311.
- Rice, J. R. (2006). Heating and weakening of faults during earthquake slip, *J. Geophys. Res.* **111,** no. B5, doi: 10.1029/2005JB004006.

- Rice, J. R. (2017). Heating, weakening and shear localization in earthquake rupture, *Phil. Trans. Roy. Soc. Lond. A* **375**, 20160015, doi: 10.1098/rsta.2016.0015.
- Richardson, R. M., and S. C. Solomon (1977). Apparent stress and stress drop for intraplate earthquakes and tectonic stress in the plates, *Pure Appl. Geophys.* **115**, 317–331.
- Shearer, P. M., G. A. Prieto, and E. Hauksson (2006). Comprehensive analysis of earthquake source spectra in southern California, *J. Geophys. Res.* **111,** no. B6, doi: 10.1029/2005JB003979.
- Shipton, Z. K., A. M. Soden, J. D. Kirkpatrick, A. M. Bright, and R. J. Lunn (2006). How thick is a fault? Fault displacement-thickness scaling revisited, in *Earthquakes: Radiated Energy and the Physics of Faulting*, R. Abercrombie, A. McGarr, G. DiToro, and H. Kanamori (Editors), Geophysical Monograph Series, Vol. 170, AGU/Wiley, Washington DC, 193–198.
- Sibson, R. H. (1973). Interactions between temperature and pore-fluid pressure during earthquake faulting and a mechanism for partial or total stress relief, *Nature* **243**, no. 126, 66–68.
- Stein, R. S., and P. Bird (2024). Why do great continental transform earthquakes nucleate on branch faults? *Seismol. Res. Lett.* (submitted May 2024 to the Kagan/Jackson memorial volume) (under review).
- Storchak, D. A., J. Harris, L. Brown, K. Lieser, B. Shumba, and D. Di Giacomo (2020). Rebuild of the Bulletin of the International Seismological Centre (ISC)—Part 2: 1980–2010, *Geosci. Lett.* 7, no. 18, doi: 10.1186/s40562-020-00164-6.
- Storchak, D. A., J. Harris, L. Brown, K. Lieser, B. Shumba, R. Verney, D. Di Giacomo, and E. I. M. Korger (2017). Rebuild of the Bulletin of the International Seismological Centre (ISC), part 1: 1964–1979, *Geosci. Lett.* 4, no. 32, doi: 10.1186/s40562-017-0098-z.
- Styron, R., and M. Pagani (2020). The GEM Global active faults database, *Earthq. Spectra* **36**, no. 1, 160–180, doi: 10.1177/8755293020944182.

Manuscript received 2 May 2024 Published online 21 August 2024